

A060443

Naval Air Systems Command

Contract N00019-77-C-0293

STUDIES OF EXTINCTION BY SMALL PARTICLES IN THE
10 MICRON SPECTRAL REGION

Jul 8 1978

42p.

Donald R. Huffman
Department of Physics
University of Arizona
Tucson, Arizona 85721

Best Available Copy

DDC
RECEIVED
OCT 30 1978
RECEIVED
D

APPROVED FOR PUBLIC RELEASE
DISTRIBUTION UNLIMITED

78 10

**Best
Available
Copy**

12

DISTRIBUTION STATEMENT A
Approved for public release;
Distribution Unlimited

DDC
RECEIVED
OCT 30 1978
RECEIVED

These were considered to be good candidates for producing appreciable attenuation of the CO₂ laser wavelengths for two different reasons relating to the processes involved in stopping a beam of light. These two processes are scattering of light out of the beam and absorption of light within the particles, the sum of these stopping processes being known as extinction.

$$\text{extinction} = \text{absorption} + \text{scattering}$$

(Mathematical expressions for these quantities will be given in Section II.) The glass bubbles, already available commercially, were expected to give large extinction by the scattering process since the effective sizes are approximately equal to the infrared laser wavelengths. Because of the thin-walled nature of the bubbles, the mass per unit of extinction would be kept low; that is, the bubbles were expected to provide high extinction per unit mass by way of their scattering properties. The silicate smoke particles, on the other hand, were known to have quite high absorption efficiencies in the vicinity of 10 μm wavelength.

For the purpose of determining the infrared extinction from the two types of particles, two approaches may be used. The extinction may be calculated from known optical properties of the solids, or the attenuation of light through a collection of the particles can be measured directly. One advantage of the calculations is that other parameters such as size distribution can be easily changed in the calculations, while the experimental technique is limited to the specific sizes of particles available or produceable. The calculations, however, are fairly difficult and input parameters such as optical properties and

appropriate size distributions must be experimentally determined. Also, the calculations can only be accomplished for ideal geometries such as spheres or spherical shells. The applicability of these calculations to other shapes needs to be examined by comparison with measurements.

The plan of this work has been to determine optical constants and size distributions necessary for doing theoretical calculations of extinction for both kinds of particles. Extinction measurements are made to determine the validity of the calculations. Recommendations can then be made based on the comparison of results for the two types of particles. Finally, the most promising parameters can then be predicted from the calculations.

B. Limitations of this Work

This work will be restricted to the two representative types of particles -- glass bubbles and one of the most promising of the silicate smokes, olivine smoke. Further work on solids of different chemical composition will be left for other investigations. A further limitation is that we do not study the problem of how the particles are to be produced and dispersed as an aerosol. These may be important and difficult problems of a practical nature, especially since the extinction is known to be somewhat dependent on the degree of agglomeration of the dispersed particles.

C. Plan of the Presentation

This report will summarize the research methods used and the results obtained during the past year under the support of NASC contract N00019-77-C-0293.

The next section (II) will summarize the necessary theory by way of the main equations used in the scattering theory for spherical particles and spherical shells, and theory needed to analyze specular reflectance data from solids to determine complex optical constants. An exhaustive treatment of this theory is not necessary here since it is covered in various readily-available references. The summary of the main equations is desirable, however, in order to clearly define the terms used and to explain the methods. Following the theory section, results of measurements and calculations on each of the two particulate systems, glass spheres and silicate smokes, will be presented in turn (Sections III and IV respectively). Each of these sections will include the necessary discussions of optical constants determinations, particle size distributions, extinction calculations, and extinction measurements. Section V will then compare the resulting extinction spectra for the two particulate systems, and will present conclusions based on this work.

II. THEORY

A. Theory of Extinction

A well defined beam of light, such as a laser beam, is attenuated as it passes through a collection of particles. The attenuation is caused by two processes -- scattering away from the original direction by the particles, and absorption of light within the particles with subsequent conversion of the photon energy into heat. The transmission I/I_0 of a beam of light having initial intensity I_0 and final intensity I after traversing a distance l through a collection of uniformly dispersed, randomly oriented particles can be written as follows:

$$I/I_0 = \exp (-N\sigma_{\text{ext}}) l \cdot \quad (\text{II-1})$$

N is the number of particles per unit volume in the light path and σ_{ext} is the cross section for the extinction process, which can be separated into the separate scattering and absorption parts

$$\sigma_{\text{ext}} = \sigma_{\text{sca}} + \sigma_{\text{abs}}$$

The major computational problem in calculating extinction by particles is to determine the extinction cross sections, σ_{ext} . In general this involves a solution to the electromagnetic boundary value problem, which is quite untenable in the cases of particles having arbitrary shapes and arbitrary sizes. The solution to this problem for the special case of spherical particles was developed early in the present century by Mie (1908) and by Debye (1909), generally referred to as Mie theory. The equations for their solution are complicated but are nicely given in a number of more modern references (Stratton 1941, van de Hulst 1957, Kerker 1969). The necessary input parameters are

the wavelength of the light - λ ,

the particle radius - r ,

and the complex index of refraction for the solid at the wavelength - $m = n + ik$.

In recent years high speed digital computer techniques have permitted the Mie equations to be readily solved. In this work a Fortran program based on work by Dave (1968) has been used.

The boundary value problem for concentric spheres was solved much later (Güttler 1952). The equations are more complicated and consequently the computer program is more difficult, but similar solutions exist. The required input parameters are similar except of course that both inner and outer sphere radii must be included, and separate optical constants must be supplied for

78 10 16. 0

the inner sphere and the outer sphere. In this work, the inner sphere was always considered to be empty space ($m = 1.0 + i0.0$), and the outer shell was glass, with optical constants measured in this work.

For non-spherical particles there are no general solutions for arbitrary-sized particles. A sometimes useful approximation can be obtained for ellipsoidal particles in the so-called Rayleigh limit (where the size of the particle and its optical dimensions, $n \times \text{length}$, are very small compared to the wavelength). Using this approximation one can sometimes get insights into the effect of varying shapes. Usually, one assumes that the spherical approximation applies reasonably well to non-spherical particles also, but it is well to continually remember that this assumption is being made. Reference to experimental measurements on real (frequently non-spherical) particles is then a good idea for delineating the limits of validity of the simplifying approximation. This is the approach we have used in this work. All calculations presented are for the spherically symmetric cases -- spheres and concentric spheres.

For the cases of spheres or spherical shells, the light beam transmission through a path length ℓ can be written.

$$\begin{aligned} I/I_0 &= \exp(-NQ_{\text{ext}} \pi r^2) \ell \\ &= \exp\left(-\frac{n}{V} Q_{\text{ext}} \pi r^2\right) \ell \end{aligned} \quad (\text{II-2})$$

where $Q_{\text{ext}} = Q_{\text{sca}} + Q_{\text{abs}}$. The Q 's are known as efficiency factors for spheres which are obviously transformed into cross sections by multiplication by the cross sectional area of a sphere, πr^2 . N is the number of particles per unit volume, n/V . Although this expression is quite acceptable for calculations, it is sometimes useful to relate the transmission to the mass concentration of particles c (mass of particulates per unit volume of space). For a monodisperse (single size) collection of particles,

$$c = \frac{m}{V} = \frac{n \frac{4}{3} \pi r^3 \rho}{V} \quad (II-3)$$

where

n = number of particles in volume V

r = particle radius

ρ = mass density of particulate material.

It follows simply that

$$\frac{n}{V} = \frac{c}{\frac{4}{3} \pi r^3 \rho}$$

which is put into Eq. (II-2) to yield

$$I/I_0 = \exp \left(- \frac{c}{\frac{4}{3} \pi r^3} Q \pi r^2 \right) \ell \quad (II-4)$$

$$= \exp \left(- \alpha_p \right) \frac{c}{\rho} \ell \quad (II-5)$$

$$= \exp \left(- \alpha_p \right) \frac{c}{\rho} \quad (II-6)$$

in which σ is the mass/area of particles.

The extinction cross section per unit volume of the solid, α_p , is defined by Eq. (II-5) and is related to the extinction efficiency factor for spheres, Q_{ext} , by comparison with (II-4) as follows:

$$\alpha_p = \frac{Q \pi r^2}{\frac{4}{3} \pi r^3} = 3/4 \frac{Q_{ext}}{r} \quad (II-7)$$

Many authors prefer to calculate extinction cross sections normalized per unit mass of the solid material, α , sometimes referred as the mass extinction coefficient. This is simply related to our α_p by the solid density,

$$\alpha = \frac{\alpha_p}{\rho} = 3/4 \frac{Q_{ext}}{\rho r} \quad (II-8)$$

with the corresponding transmission equation being

$$I/I_0 = \exp (- \alpha c \ell) \quad (II-9)$$

By measuring the mass density of particles collected on a filter or substrate (σ) and the transmission through the coated substrate (I/I_0), and using Eq. (II-6), the α_p 's can be determined experimentally, leading to an experimental determination of Q_{ext} for spheres from Eq. (II-6). These equations provide the connection between theory and experiment for mono-dispersed collections of particles.

If there is a size distribution of spheres, the volume-normalized extinction cross section is determined from the particle size distribution function $N(r)$ as

$$\alpha_p = \frac{\int N(r) Q(r) \pi r^2 dr}{\int N(r) \frac{4}{3} \pi r^3 dr} \quad (\text{II-10})$$

rather than Eq. (II-7). $N(r)$ is the number per unit volume of particles having radii between r and $r + dr$.

In the case of spherical shells, once the Q 's have been calculated, the α_p 's are determined through division by the volume of the shell (rather than of the sphere) or by the volume distribution of the shells as follows:

$$\alpha_p = \frac{Q \pi r^2}{\frac{4}{3} \pi (r_o^3 - r_i^3)} = \frac{Q \pi r^2}{\frac{4}{3} \pi r_o^3 [1 - (r_i/r_o)^3]} \quad (\text{II-11})$$

$$\frac{\int N(r_o) Q(r_o) \pi r_o^2 dr_o}{\int N(r_o) \frac{4}{3} \pi r_o^3 [1 - (r_o/r_i)^3] dr_o}, \quad (\text{II-12})$$

where r_o and r_i are the outer and inner radii of the shell respectively. Note that the radius distribution in Eq. (II-12) is over outer radii. In this work we consider the ratio of inner to outer radius to be constant.

B. Theory of Optical Constants Determinations

The non-coherent, linear optical properties of a solid are summarized by the index of refraction n and the extinction coefficient k , both of which may be strong functions of wavelength. These two quantities constitute the real and imaginary parts of the complex refractive index

$$m = n + ik \quad . \quad (II-13)$$

To avoid confusion with extinction in the sense of scattering plus absorption by small particles, the term extinction coefficient for k will not be used. A negative sign is frequently found in the complex refractive index relating to the other choice for the phase convention of a sinusoidal wave.

In regions of low absorption, such as the visible region for clear glasses, n and k are easily determined by a combination of reflectance and transmission measurements, or by a transmission measurement coupled with a measurement of minimum deviation through a prism of the material. In regions where the absorption coefficient is very high, such as near $10 \mu\text{m}$ for the silicates of concern in this work, transmission cannot be measured except on thin films. The most common measurement is almost-normal incidence reflectance over a range of wavelengths. The data are usually analyzed to obtain the optical constants by one of the following methods:

- (1) Kramers-Kronig analysis
- (2) Multiple oscillator fits to the data

The Kramers-Kronig dispersion equations relate the real and imaginary parts of any complex response function, under very general conditions (Stern 1963). A response function relates a cause to an effect. The complex amplitude reflection coefficient, $\tilde{r}(\omega) = r \exp(i\theta)$, is such a suitable response

function as is the function

$$\ln \tilde{r} = \ln r(\omega) + i\theta(\omega).$$

The Kramers Kronig relations between the real and imaginary parts of this function are given by

$$\theta(\omega) = -\frac{2\omega}{\pi} P \int_0^{\infty} \frac{\ln \tilde{r}(\omega')}{\omega'^2 - \omega^2} d\omega' \quad (\text{II-14})$$

where P denotes the principle value of the integral. This can be put in the following form used in this work:

$$\theta(\omega) = \frac{2\lambda}{\pi} \int_0^{\infty} \frac{\ln r(\lambda') - \ln r(\lambda)}{\lambda'^2 - \lambda^2} d\lambda' \quad (\text{II-15})$$

Since the magnitude of the amplitude reflection coefficient is related to the measured intensity reflection coefficient R by

$$r = \sqrt{R}, \quad (\text{II-16})$$

the θ 's can be calculated if reflectance is known. In the theory the reflectance must be known from wavelengths of 0 to ∞ , but in practice suitable extrapolations can give a good approximation to the true phase shifts θ if reflectance measurements extend a considerable distance on either side of the wavelength of interest. Once the phase shifts have been calculated at a given λ from the integral over all wavelengths, the optical constants can be calculated at this wavelength from the following expressions:

$$n(\lambda) = \frac{1 - r^2(\lambda)}{1 + r^2(\lambda) - 2r(\lambda) \cos \theta(\lambda)} \quad (\text{II-17})$$

$$k(\lambda) = \frac{2r(\lambda) \sin \theta(\lambda)}{1 + r^2(\lambda) - 2r(\lambda) \cos \theta(\lambda)} \quad (\text{II-18})$$

The exact nature of the extrapolations used and the computer program are given in Steyer (1974).

The second method for analyzing reflectance data for optical constants is to assume the oscillators responsible obey a multiple, Lorentzian oscillator theory. This is known to be the case to a close approximation for many simple solids in the infrared lattice vibration region. In the Lorentzian model the complex dielectric function is given by

$$\epsilon^* = \epsilon_1 + i\epsilon_2 = \epsilon_\infty + \sum_j \frac{f_j \omega_j^2}{\omega_j^2 - \omega^2 + i\omega\Gamma_j} \quad (\text{II-19})$$

where the parameters ω_j , Γ_j , and f_j determine the position, width, and strength of the j th oscillator, and ϵ_∞ is the high frequency dielectric function (visible frequencies in this work). The optical constants are related to ϵ_1 and ϵ_2 by

$$\epsilon_1 = n^2 - k^2 \quad (\text{II-20})$$

$$\epsilon_2 = 2nk$$

and the normal incidence reflectance is given by

$$R = \frac{(n-1)^2 + k^2}{(n+1)^2 + k^2} \quad (\text{II-21})$$

Optical constants are derived from the data by repeatedly varying the oscillator parameters and calculating reflectance spectra until a good fit is obtained to the measured reflectance spectrum. The oscillator parameters so determined produce the required optical constants.

In this work the Kramers-Kronig technique was used, except in the case of amorphous olivine material produced by radiation damage. In this case an oscillator fit was easier, since the radiation resulted in a thin, amorphous layer on top of a crystalline bulk having previously-determined oscillator parameters.

III. GLASS BUBBLES

The thin-walled glass bubbles or micro-balloons used in these studies were acquired from two different manufacturers by Dr. Carl Dinerman of the Naval Weapons Support Center, Crane, Indiana. They are identified as follows:

E & C: Emerson and Cumming, Inc.
Ecospheres FTF15

3M : 3M Brand
Glass Bubbles

We will frequently use the shortened form of the names as given above. The following table summarizes the appropriate information from the respective manufacturers' specification sheets:

Table I		
<u>Properties of the Glass Bubbles</u>		
	<u>E & C</u>	<u>3M</u>
Reference	Tech. Bull. 14-2-4D	Technical Data 1
Particle size range	2 to 44 μm	
True Density (liquid displacement)	.28 to .32 gm/cm^3	
Type of material	insoluble glass	similar to window glass
Inner/outer radii (calculated from density)	.96	

A. Size Distributions

In order to proceed with computer calculations of extinction, it is necessary to have more complete size information (distribution of inside and outside radii). For this purpose both light microscopy and scanning electron microscopy were completed for both samples of bubbles. Examples of the photomicrographs are shown in Figs. 1 through 5.

Figs. 1 and 2 are light micrographs of the two types of bubbles. These pictures have been used to determine size distributions for the particles. Measurements of individual particle diameters were fed into a simple statistics program to determine the properties of the size distributions which are summarized in Fig. 6. The mean sizes are essentially the same for bubbles from the two manufacturers -- 19 μm . The size distributions summarized by the two histograms are slightly different. We note a slight discrepancy between our mean size of 19 μm and the Emerson and Cumming statement of average size as less than 15 μm , but this difference is not expected to be important.

Figs. 4 and 5 show an interesting case of a broken bubble as viewed by the scanning electron microscope. Fig. 5 permits a rather accurate measurement to be taken of the shell thickness in comparison to the outer diameter. From this case we have determined that the ratio of inner to outer radius is $r_i/r_o = 0.96$ which is in excellent agreement with the value determined from the true density as quoted by E & C. Because of the difficulty of determining shell thicknesses and the complexity of including differing distributions of inner and outer radii we have chosen to consider the above ratio of r_i/r_o to be representative of the bubbles, independent of outer radius distribution. This fact, along with the distribution of r_o specifies the geometrical parameters needed for the calculations.

B. Measurements of Optical Constants

In the vicinity of 10 μm all silicate materials have very strong absorption bands due to interaction of the light with the stretching

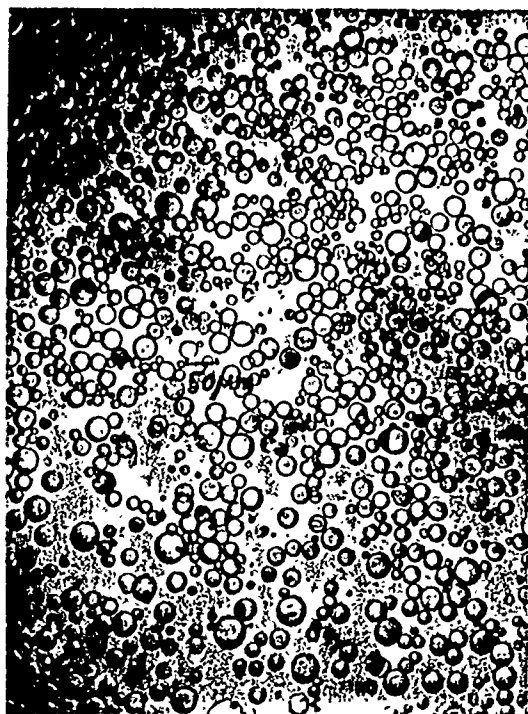


Figure 1

Emerson and Cumming glass bubbles
taken with the light microscope

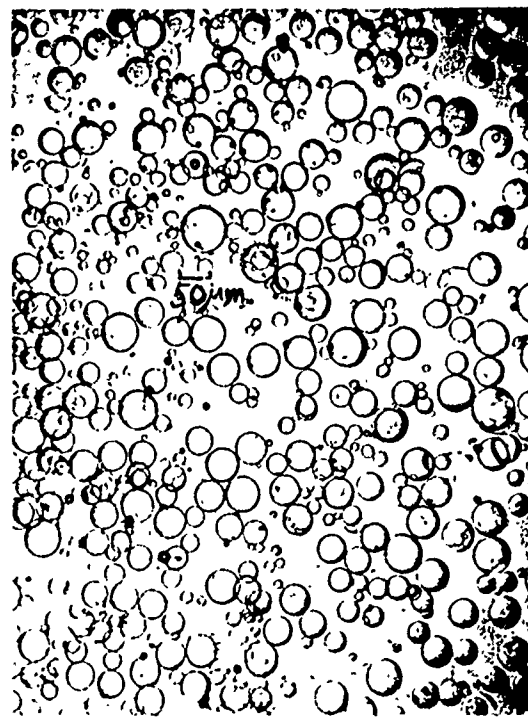


Figure 2

3M glass bubbles taken with
the light microscope

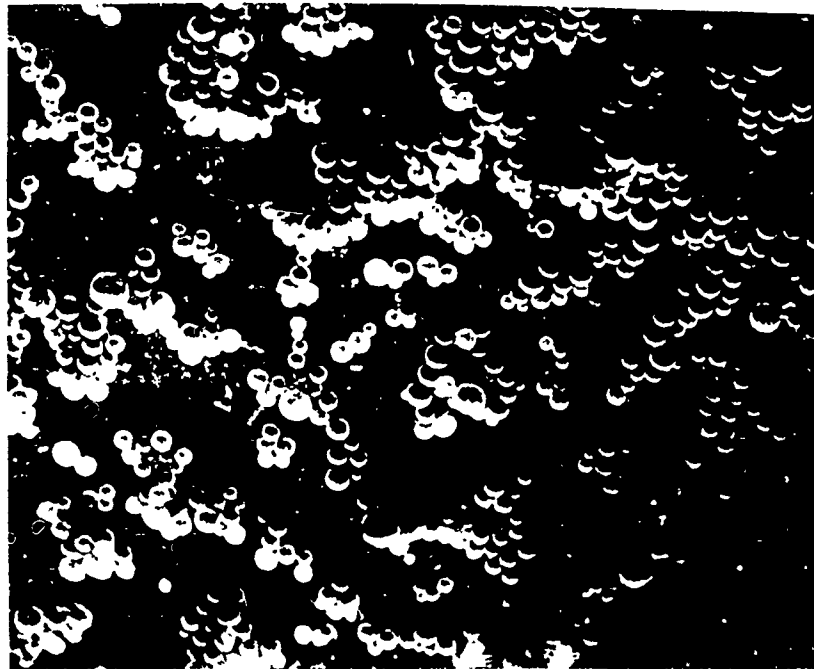


Figure 3

Emerson and Cumming glass bubbles taken with the scanning electron
microscope ($\sim 200\times$)

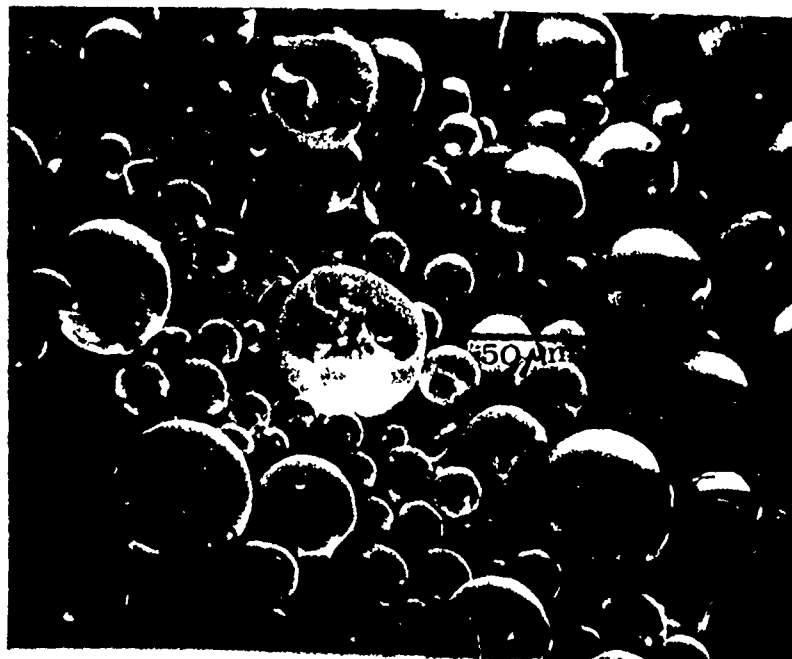


Figure 4

3M glass bubbles taken with the scanning electron microscope
(~500x)



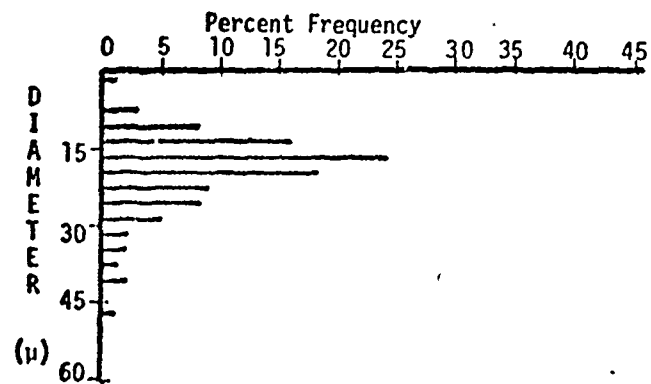
Figure 5

3M glass bubbles showing a broken bubble. The thickness
of the shell can be determined at several points.

EMERSON AND CUMMINGS GLASS BUBBLES

Average diameter 19.2 μ

Standard deviation 7.2 μ



3M GLASS BUBBLES

Average diameter 19.7 μ

Standard deviation 12.4 μ

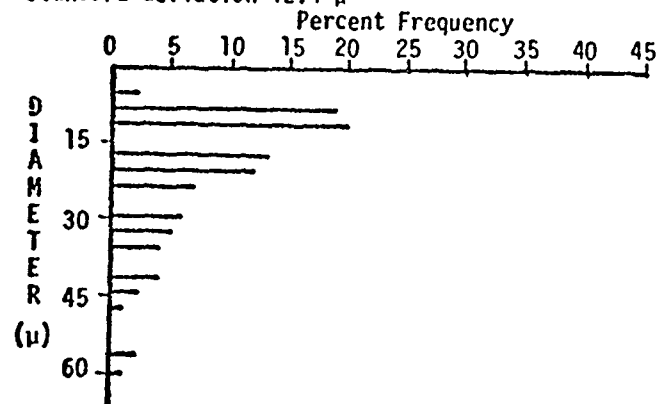


Figure 6

Size distribution histograms for the two bubble materials taken from photomicrographs.

modes of vibration of the Si-O bonds. This is an example of a situation where optical constants are most easily derived from reflectance spectra measured at near-normal incidence from a polished surface of bulk material and use of the Kramers-Kronig analysis. This is the technique we have used to determine optical constants of the two bubble glasses.

Toward this end it was necessary to melt the bubble material into a homogeneous mass. This apparently simple task proved to be one of the greatest challenges in the entire project. Simple heating of the compacted material to 1300 °C failed to cause them to flow into anything like a clear mass. After trying various techniques it was found that an oxy-hydrogen torch, carefully played over a pile of the bubbles on a carbon block could melt the material into relatively gas-bubble-free pieces of about 5 mm or more across. The two bubble materials behaved quite differently under the flame, however. Gentle heating (to perhaps 600 °C) of the 3M bubbles caused the material to slowly fuse and release most of the trapped gases. The E & C bubble material had to be heated to a white hot heat (an estimated 1300 °C) before fusion into one molten lump could be accomplished. This fact led us to believe that the E & C glass was probably quite similar to fused silica, although the manufacturer only states that it is "insoluble glass".

In order to provide further information on the nature of the glasses, refractive index (n) measurements were carried out at several visible wavelengths. The determination was made by the method of minimum deviation through a prism (see for example Jenkins and White 1957). Two flat faces were ground and polished on samples of the fused glasses. The angle of minimum deviation through each prism and the prism angles were measured with a mechanical spectroscope that could be read to $\frac{1}{2}$ minute of an arc ($.008^\circ$), fitted with a crystal-orientating goniometer. Results

calculated from these data for n at several wavelengths in the visible are shown in Table II below.

Table II
Measured Refractive Indices in the Visible for the Two
Bubble Materials and for Fused Silica

<u>Wavelength</u>	<u>Fused Silica</u>	<u>E & C</u>	<u>3M</u>
.63 $m\mu$	1.4572	1.4572 \pm .0005	1.504 \pm .005
.59	1.4584	1.4586 "	
.56	1.4596	1.4596 "	1.494 \pm .01
.44	1.4664	1.4660 "	1.508 \pm .01

The larger experimental uncertainties in the case of the 3M material was due to the lack of transparency in this sample because of included gas bubbles. It is apparent from the results that the E & C material after being fused by our technique is optically similar to fused silica within narrow limits. This confirms the chemical similarity to silica already observed in the melting studies. On this basis the early progress reports of this work used published optical constants in the 10 μ m region for silica in calculating extinction of bubble material. The 3M material after being fused by our technique is quite different in refractive index, being fairly near to values quoted for borosilicate crown glass.

Reflectance measurements on polished faces of the two fused bubble materials were measured from 3 μ m to 25 μ m. The almost-normal incidence measurements were taken with two specular reflectance attachments fitted

into a Perkin Elmer 337 and a Beckman IR12 spectrophotometer. An aluminum reflectance standard was used in a sample-in-standard-in method. Resulting reflectance spectra in the $7\mu\text{m}$ to $25\mu\text{m}$ region for the two materials and for fused silica are presented in Fig. 7. Again one observes that the E & C material is quite similar to fused silica except for the magnitudes of the reflectance peaks, while the 3M material is considerably different. Complex indices of refraction derived from the reflectance measurements by the Kramers-Kronig computer program are summarized in Table III.

Table III
Complex Optical Constants for the Two Bubble Materials
and for Fused Silica

λ	<u>Fused Silica</u>		<u>E & C Material</u>		<u>3M Material</u>	
	<u>n</u>	<u>k</u>	<u>n</u>	<u>k</u>	<u>n</u>	<u>k</u>
7.8			.64	.09	.88	.18
8.0	.48	.18	.46	.39	.75	.25
8.2	.38	.55	.48	.55	.68	.41
8.4	.46	.80	.49	.73	.64	.59
8.6	.45	.94	.49	.95	.65	.77
8.8	.39	1.37	.50	1.16	.65	.93
9.0	.68	2.31	.69	1.63	.75	1.25
9.2	1.72	2.51	1.07	1.82	.94	1.41
9.4	2.73	1.71	1.51	1.83	1.31	1.59
9.6	2.89	1.03	2.09	1.55	1.61	1.59
9.8	2.76	.54	2.25	1.20	1.84	1.59
10.0	2.40	.22	2.24	.93	2.13	1.24
10.4	2.01	.14	2.15	.57	2.21	.82
10.8	1.82	.10	1.99	.43	2.17	.61
11.2	1.72	.14	1.89	.35		
11.4	1.69	.16	1.80	.33	2.09	.39
12.1	1.66	.26	1.66	.37	1.84	.30

These constitute the optical parameters required as input for the extinction calculations.

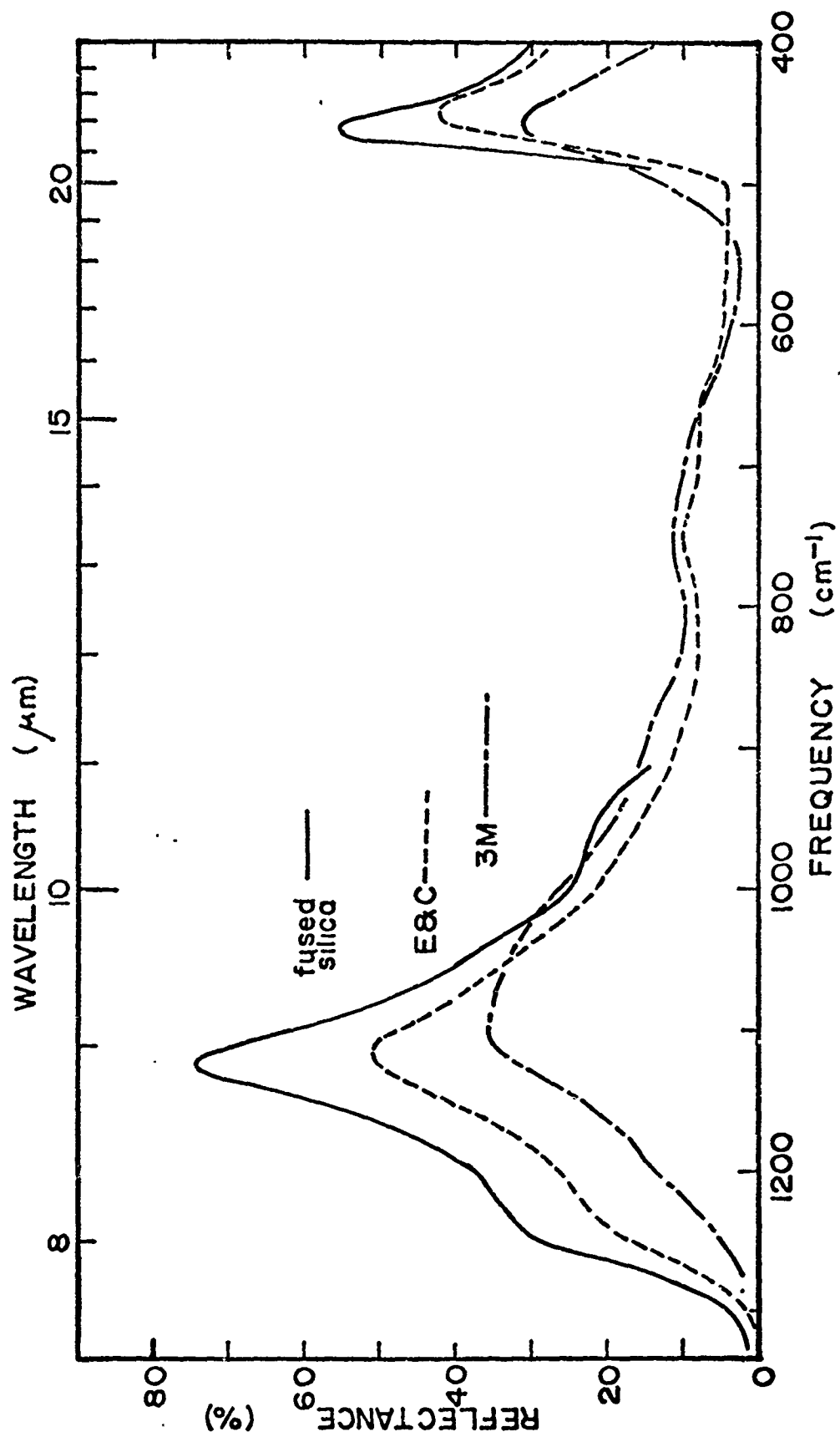


Figure 7
Reflectance spectra of the three bulk materials -- fused silica,
E & C bubble material, and 3M bubble material.

C. Extinction Calculations

Using the two sets of measured bubble parameters (size distributions and complex refractive indices) presented in the previous two sections as input for the concentric spheres computer program, extinction was calculated. Size distributions used were those of Fig. 6 for outer radii, with the inner radii set by the assumption that $r_i/r_o = 0.96$, and optical constants used were from Table III. Results are shown in Fig. 8. The particular wavelengths of interest are those in the 9.6 and 10.6 μm CO_2 laser bands sketched in at the bottom of the curve from one laser manufacturer's specifications. Generally speaking the volume normalized extinction cross sections are 0.8 to $1.0 \times 10^4 \text{ cm}^{-1}$ in both bands, for both materials. In some sense Fig. 8 summarizes the final conclusions of this work as it regards the specific glass bubble samples at our disposal. However, some further insight can be obtained into the mechanisms responsible for the extinction by avoiding the complexity of the complete size distribution to examine extinction by different single sizes. This insight may provide the basis for optimizing the extinction efficiency.

An important question in this connection is how does the extinction efficiency vary with bubble size. To illustrate this, we have made a series of calculations at the fixed wavelength of 10 μm (near the maximum extinction in both materials) for a series of increasing bubble radii, the relative shell thickness being kept constant as previously ($r_i/r_o = 0.96$). The results are shown in Fig. 9. One observes, perhaps surprisingly, that the smaller bubbles are the more effective. There is no peak in the

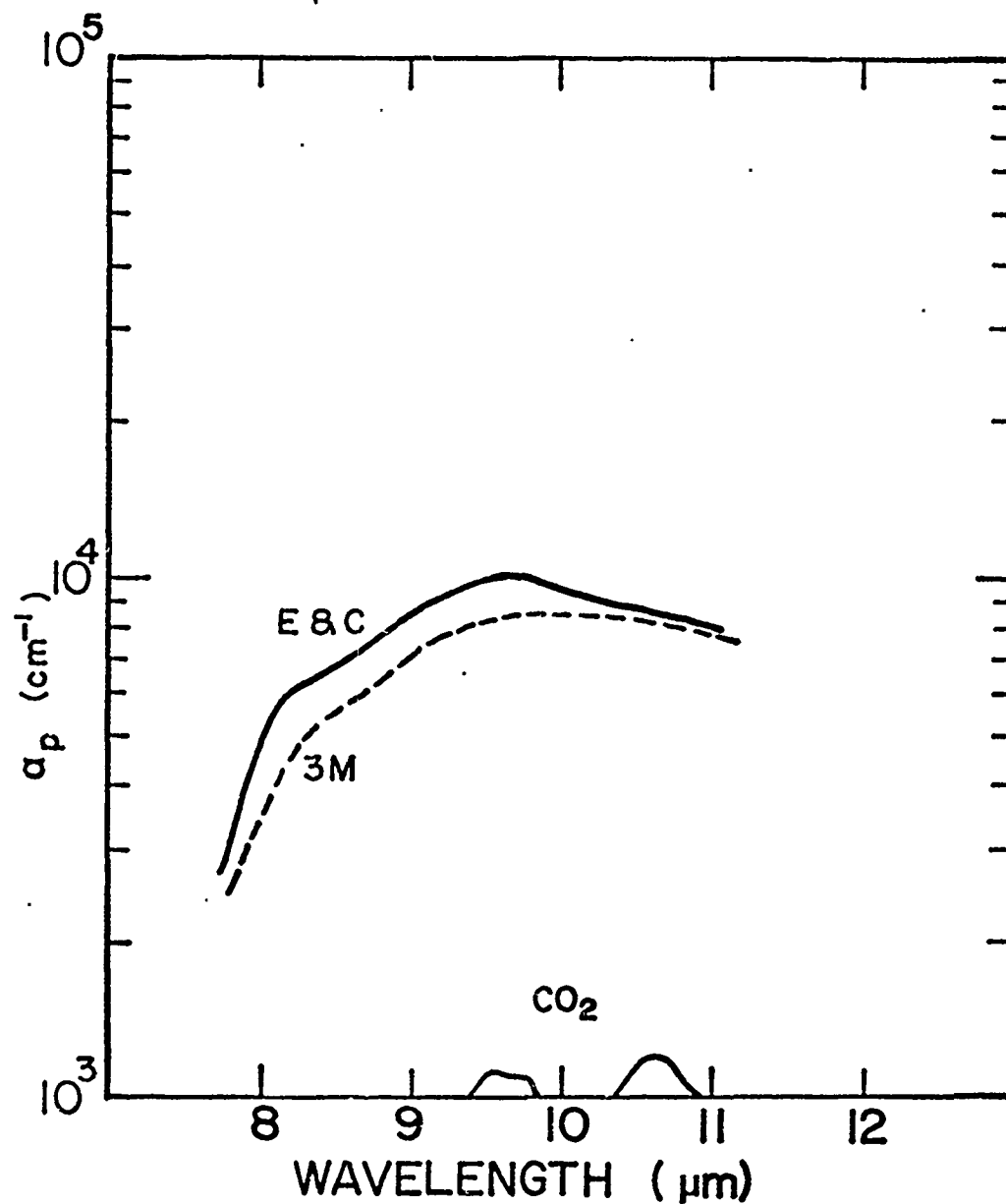


Figure 8
Extinction normalized per unit volume of solid for the
& C bubbles and for the 3M bubbles, calculated
using measured size distributions and optical
constants.

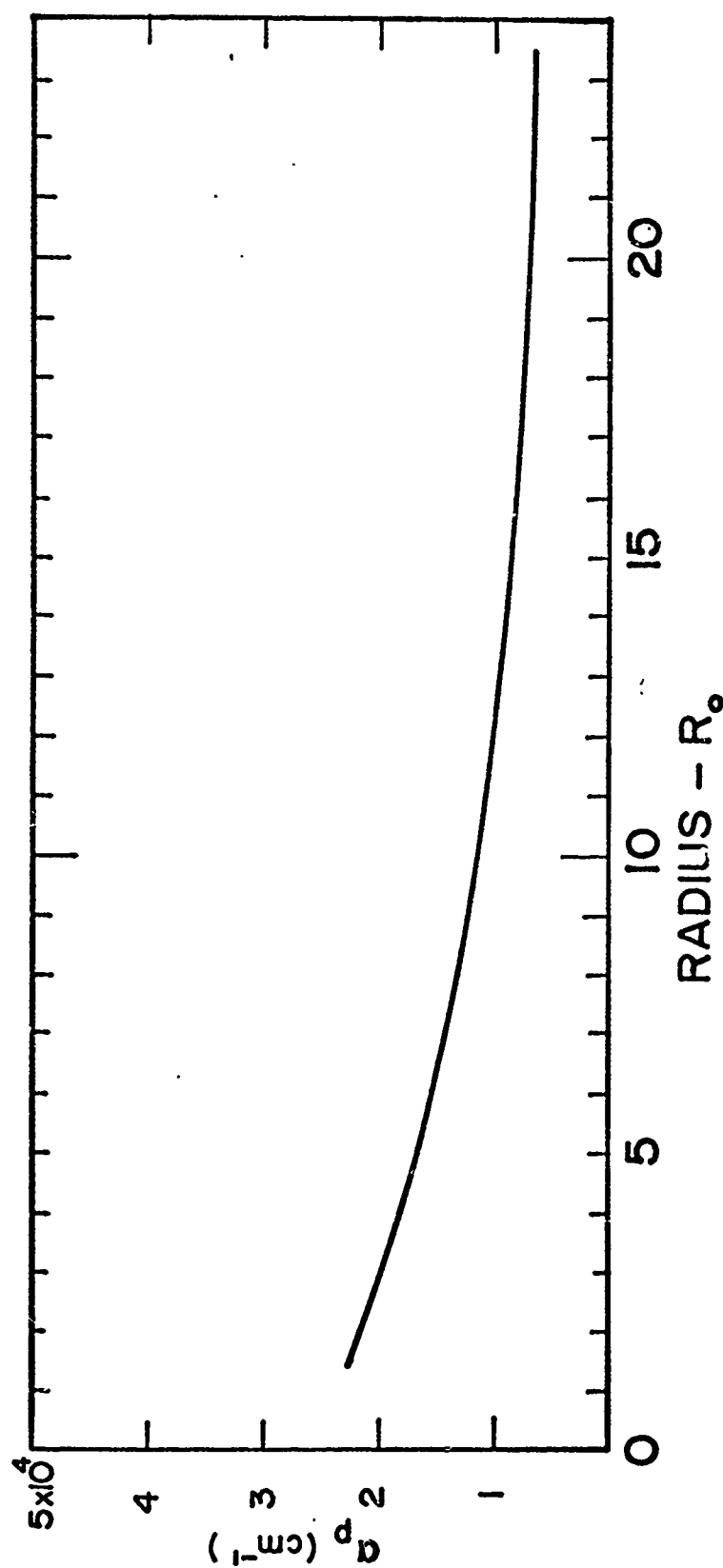


Figure 9
 Extinction normalized per unit volume of solid calculated for
 different outside radii of 3M bubbles with
 $r_i/r_o = 0.96$.

extinction efficiency as the size approaches the wavelength as there would be if the optical constants were indeed constant, and if k were small. The fact is that the large variations in optical constants in the Si-O resonance region produce strong absorption which is more important than the scattering. Table IV shows how the extinction efficiency factor is distributed between scattering and absorption efficiencies.

Table IV
Scattering and Absorption Contributions to Extinction
for 3M Glass Bubbles ($r_o = 5 \mu\text{m}$, $r_i = 4.8 \mu\text{m}$)

$\lambda(\mu\text{m})$	Q_{ext}	Q_{sca}	Q_{abs}
9.1	.76	.17	.59
9.3	.96	.22	.73
9.6	1.21	.30	.91
10.0	1.29	.35	.94
10.5	1.08	.33	.75
11.1	.77	.25	.51

One sees that absorption is the more important contribution to extinction even though the particle size is comparable to the wavelength. Furthermore, since absorption is more important, the extinction per unit volume of glass increases as the effective thickness of the glass decreases. This is an example of a type of absorption saturation in this strongly absorbing region (see Day, et al, 1974 for a discussion of this saturation). Once the particle absorbs essentially all the radiation falling on it (speaking rather loosely for simplicity) further increases in thickness will cause little increase in extinction, though the volume (and mass) will increase substantially. Thus the volume- or mass- normalized extinction must decrease as the effective absorbing thickness increases. The

conclusion must follow that the smaller bubbles, having smaller wall thicknesses, are the more effective. An obvious improvement in extinction could therefore be affected by using smaller size fractions of the bubbles. With this in mind we have calculated the extinction spectrum for 5 μm radius bubbles (again with $r_i/r_o = 0.96$) with optical constants appropriate to fused silica, 3M material, and E & C material. Fig. 10 presents the results. One notices the expected increase of maximum α_p by a factor of about 2. Of course this increased extinction efficiency for silicate glass materials theoretically could be enhanced even more by dispersing the glass as very fine particles. To illustrate this we have included in Fig. 10 the results of one Mie calculation (which is practically identical to a Rayleigh calculation for this size) for .02 μm radius E & C spheres. There is a further enhancement of extinction, although the peak has shifted to about 8.8 μm . This case illustrates the maximum, volume normalized extinction that could be expected for any kind of particles made from the 3M bubble material. In such a hypothetical case, however, we have gotten away from the original idea of scattering glass bubbles and are considering a smoke of silicate glass such as will be considered in the next section.

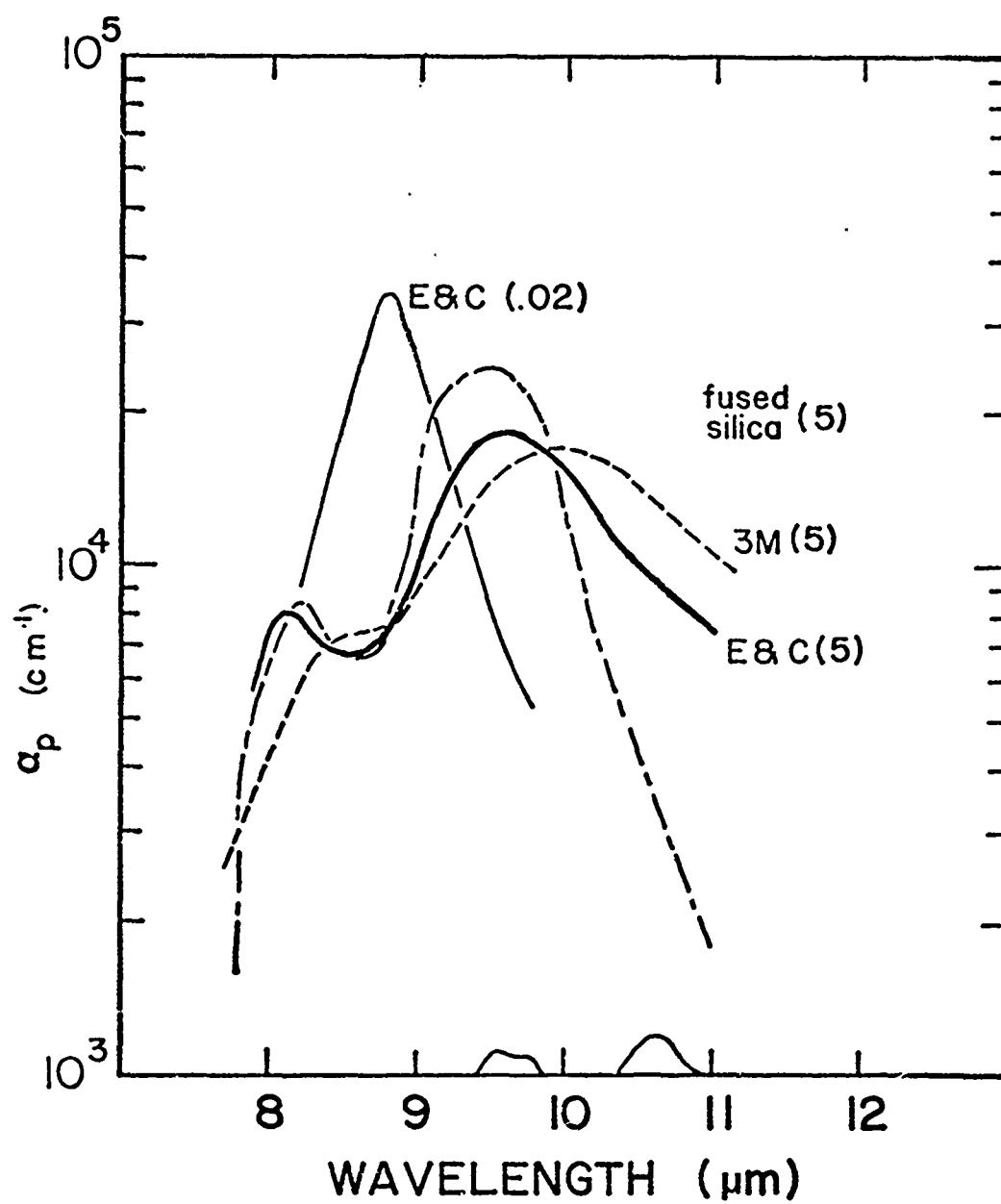


Figure 10

Extinction normalized per unit volume of the solid calculated for 5 μm bubbles of the three materials. Also shown is a calculation for .02 μm solid spheres of the E & C material.

IV. SILICATE SMOKE

In the proposal for this contract the author suggested very small particles (.01 to $0.5 \mu\text{m}$) of silicate materials, called here silicate smokes, as effective agents for extinction of CO_2 laser radiation. This suggestion was based on previous work done in this laboratory in investigation of possible interstellar grain materials which have a strong extinction "bump" in the $10 \mu\text{m}$ spectral region. This has been attributed to absorption caused by the Si-O vibration modes in silicates. (For a review of interstellar grains and optical studies of small particles see Huffman 1977). Theoretical extinction based on measured optical constants had shown volume extinction coefficients approaching 10^5 cm^{-1} . The particular one of many possible silicates suggested was the mineral olivine, $(\text{Mg,Fe})_2\text{SiO}_4$, for the following two reasons:

(1) Olivine re-condenses without decomposition after being vaporized to form smoke.

(2) It has several major absorption peaks near 9.6 and $10.6 \mu\text{m}$.

After the work got under way it became apparent that the olivine smoke sometimes condenses as crystalline particles and other times as amorphous particles. The two forms have significantly different infrared properties. Although the optical constants of crystalline olivine had already been determined in this laboratory (Steyer 1974), amorphous olivine had not been measured, and there were serious difficulties standing in the way of doing it. Apparently no one had been able to produce large (cm-sized) chunks of amorphous olivine. As do most solids, olivine much prefers to solidify in a crystalline form. The solution to the sample preparation problem came through another project in which we were exposing olivine crystals to high radiation doses of heavy ions from

a Van de Graaff accelerator, in an effort to produce astrophysically related radiation damage effects. The high degree of radiation damage produced an essentially amorphous layer on the bulk crystal. Measurements of optical constants were therefore conducted on the amorphous olivine to enable extinction calculations to be completed on this kind of particle.

The olivine smoke particles were produced by vaporizing mm-sized pieces of natural olivine from the Globe, Arizona, area. The crystal fragments are embedded in hollowed-out carbon arc electrodes, and an ac or dc arc is struck in air at a current of about 10 amp. The smoke produced as the vaporized olivine condenses was usually caught on infrared-transparent substrates of KCl or silicon for transmission measurements and for mass determinations using an analytical balance. From these results extinction (α_p) could be determined. Samples for electron microscopy were occasionally taken by placing standard electron microscope grids in the smoke stream. X-ray diffraction patterns were taken on the collected material using a powder camera. This revealed that the particles were usually highly crystalline, with identical lattice spacings to the crystal feed material. Occasionally, however, particles were produced that showed no x-ray diffraction pattern at all, and were thus concluded to be quite amorphous. The conditions for production of this amorphous material were never clearly determined, but appeared to be related to the temperatures in the condensation zone. Factors such as the shape of the electrode tips and the exact position of the molten ball of material appeared to be important variables, but these were very difficult to control in the somewhat violent process. Infrared transmission

spectra of the two smoke forms were always distinctively different in the 10 μm region. The crystalline smoke showed at least two well defined absorption peaks while the amorphous smoke showed only one broad peak.

The infrared transmission measurements taken on the smoke-coated substrates, plus mass determinations made by weighing the coated and uncoated substrates, permitted extinction coefficients to be calculated. Extinction calculations and measurements were accomplished for both crystalline and amorphous olivine smokes. These results are presented in the following section.

A. Size Distributions

Size distributions for the olivine smoke, necessary for extinction calculations, had been made in earlier studies at this laboratory (Day 1975) from electron micrographs. The particles are spherical, ranging in size from about .01 μm to about 0.2 μm radius with mean radius of about .03 μm . Since the volume normalized extinction coefficients are independent of size in the small particle, Rayleigh limit, the exact size distribution used in the calculations is immaterial and is not given in this report.

B. Optical Constants Determinations

Because of the crystalline anisotropy of olivine it is necessary that three sets of optical constants be determined -- for the electric vector of the light parallel to each of the three crystal axes. This had been done previously at this laboratory (Steyer 1974) by Kramers-Kronig analysing spectral reflectance data taken with an x-ray oriented

crystal oriented in the three different ways with respect to a polarizer in the reflectometer. Results for the optical constants of the crystalline material are shown in Fig. 11 in terms of the complex dielectric functions ϵ_1 and ϵ_2 . The dielectric functions are used here because of the simplicity of the Rayleigh extinction equation written in terms of them.

In the case of the amorphous material, optical constants were determined from the reflectance spectra of the highly disordered surface layer produced on a polished piece of single crystal olivine by ion bombardment. The polished crystal was subjected to a dose of about 5×10^{16} ions/cm² of Ne⁺ accelerated to 1.5 Mev in a Van de Graaff accelerator of the Physics Department, University of Arizona. Interference fringes in visible light determined that the damaged layer was about 2 μ m thick, in good agreement with values calculated from the expected range of such atomic particles. With our prior knowledge of the oscillator parameters necessary to describe the undamaged underlying layer, and the thickness, oscillator parameters for the damaged layer were varied until a best fit was achieved for the reflecting surface. Fig. 12 shows the measured reflectance of the undamaged and the damaged surface, along with a calculated reflectance for an infinitely thick layer of damaged material. These data are for one polarization direction of the light incident on the sample. Resulting optical dielectric functions are shown in Fig. 13 resulting from the best fit oscillator parameters. Measurements similar to those in Fig. 12 (middle) were made for the other two orientations of the major axes and optical constants derived from the best fits. The error bars in Fig. 13 represent the spread in values of ϵ_1 and ϵ_2 obtained for the three different determinations. This work is being submitted for publication (Krätschmer and Huffman 1978).

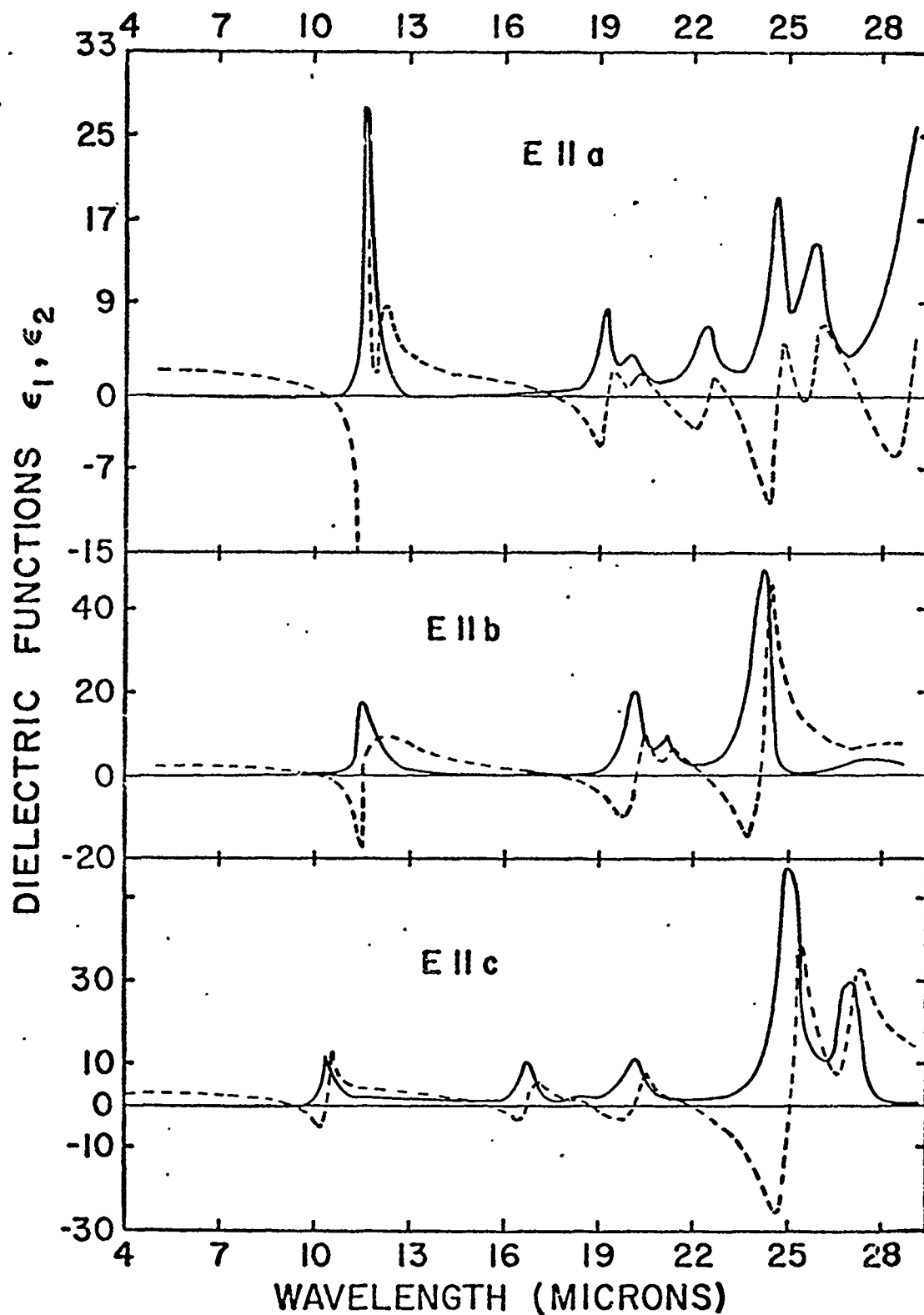


Figure 11 Dielectric functions for single crystal olivine for electric vector of the light along each of the major crystal axes - a,b,c. (from Steyer 1974)

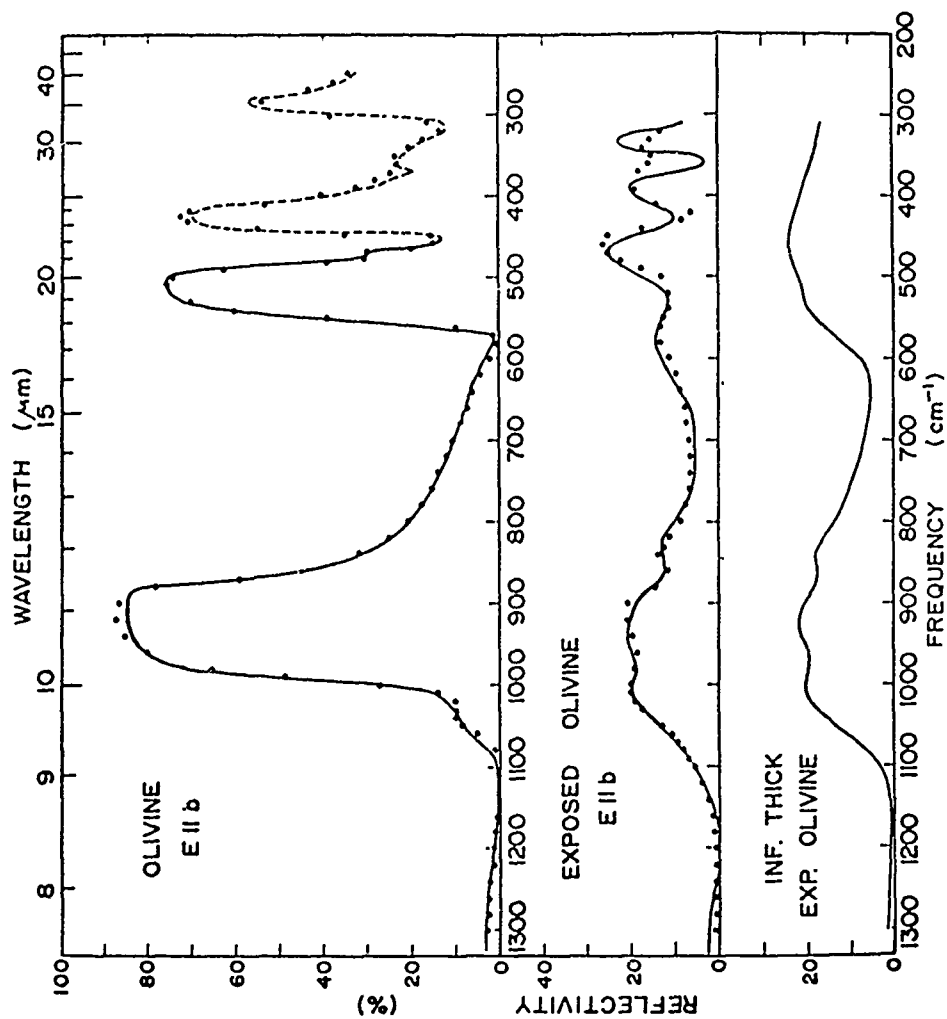


Figure 12

Reflectance measured for single crystal olivine (top) and radiation damaged olivine (middle). The bottom curve is the reflectance of an infinitely thick layer of the damaged olivine calculated from the oscillator fit.

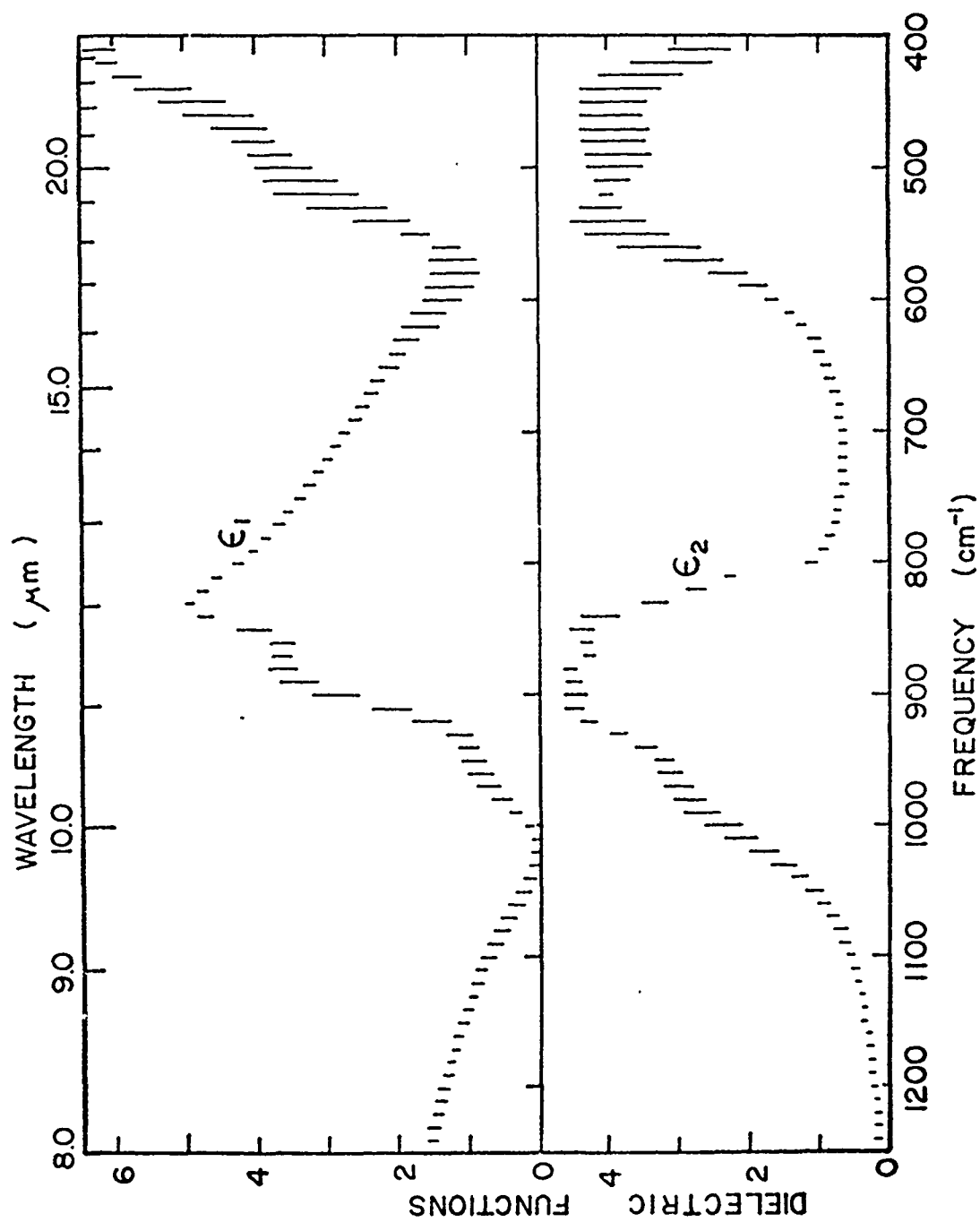


Figure 13

Complex dielectric functions for highly radiation damaged olivine, presumed to be amorphous. Error bars denote the spread in value of ϵ_1 and ϵ_2 obtained for the three orientations of the substrate.

The dielectric functions for single crystal olivine of Fig. 11 and for amorphous olivine of Fig. 13 are those used in calculations of extinction presented in the next section.

C. Extinction Measurements and Calculations

With the optical constants for crystalline and amorphous olivine taken from the preceding section, extinction calculations have been made for the two kinds of smoke. The results are shown as the solid lines in Figs. 14 and 15. The results of measurements of volume normalized extinction coefficients for the two smokes also are displayed in Figs. 14 and 15 by the dotted lines. These two figures summarize the main results of this study as it relates to the silicate smokes. Positions of the 9.6 and 10.6 μm CO_2 laser bands are shown on the figures as previously. The appearance of the extinction curves for crystalline and amorphous materials are seen to be distinctly different. There are three major peaks in the calculated extinction for crystalline smoke and one broad band for the amorphous smoke.

Some helpful insights into the nature of these extinction bands can be obtained by looking at their cause on the basis of the extinction equation for ellipsoidal particles in the Rayleigh limit ($r \ll \lambda$, $nr \ll \lambda$). The nice thing about the Rayleigh equation is that it is simple enough that one can see the effect of varying its parameters, and it is not restricted to spheres, so that insights into shape effects are possible. The extinction cross section per unit volume for an ellipsoidal particle can be written in terms of the complex dielectric function of the solid and the quantities $4\pi L_j$, known as depolarization factors in electromagnetic

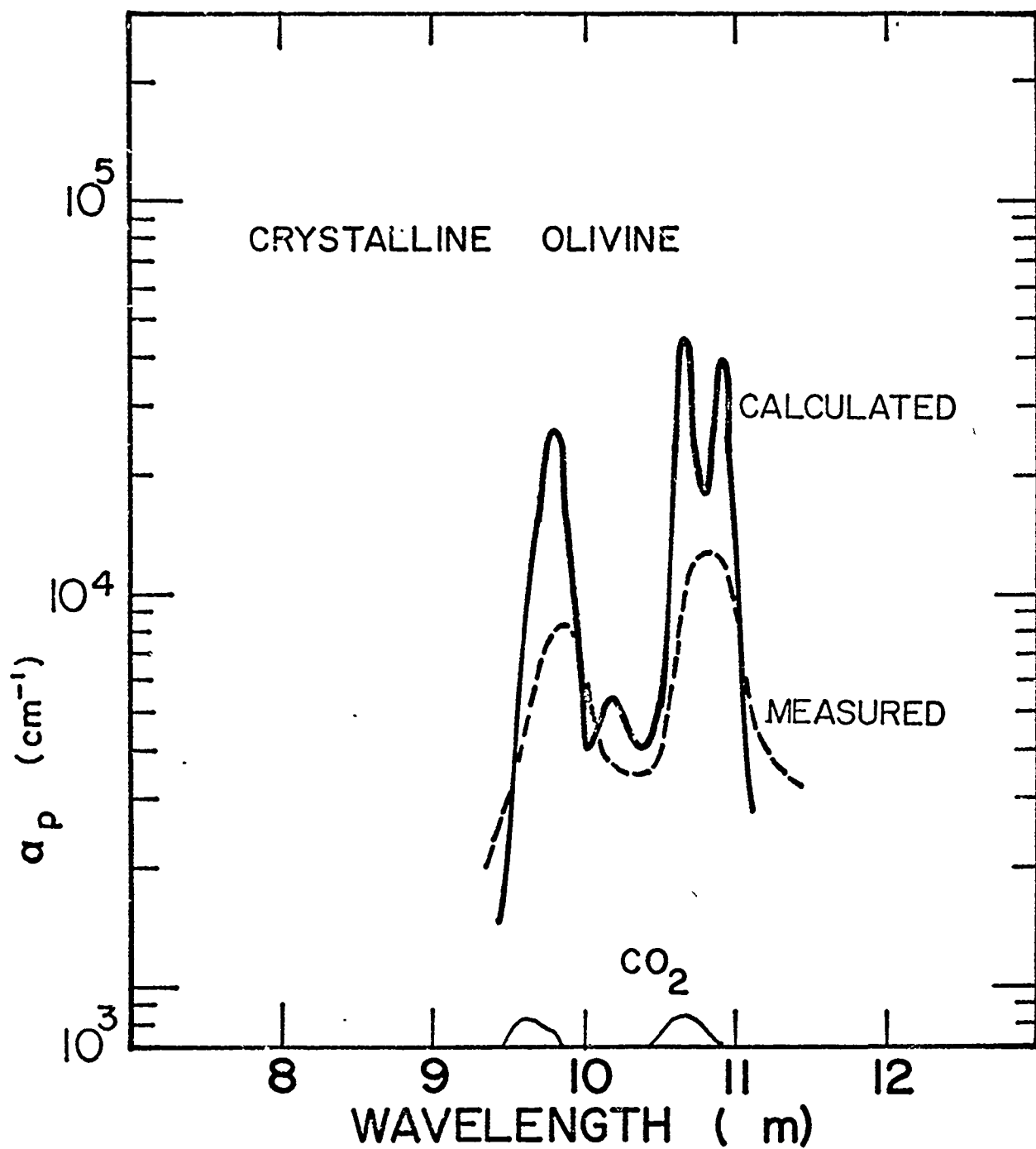


Figure 14

Measured and calculated extinction for crystalline olivine smoke.

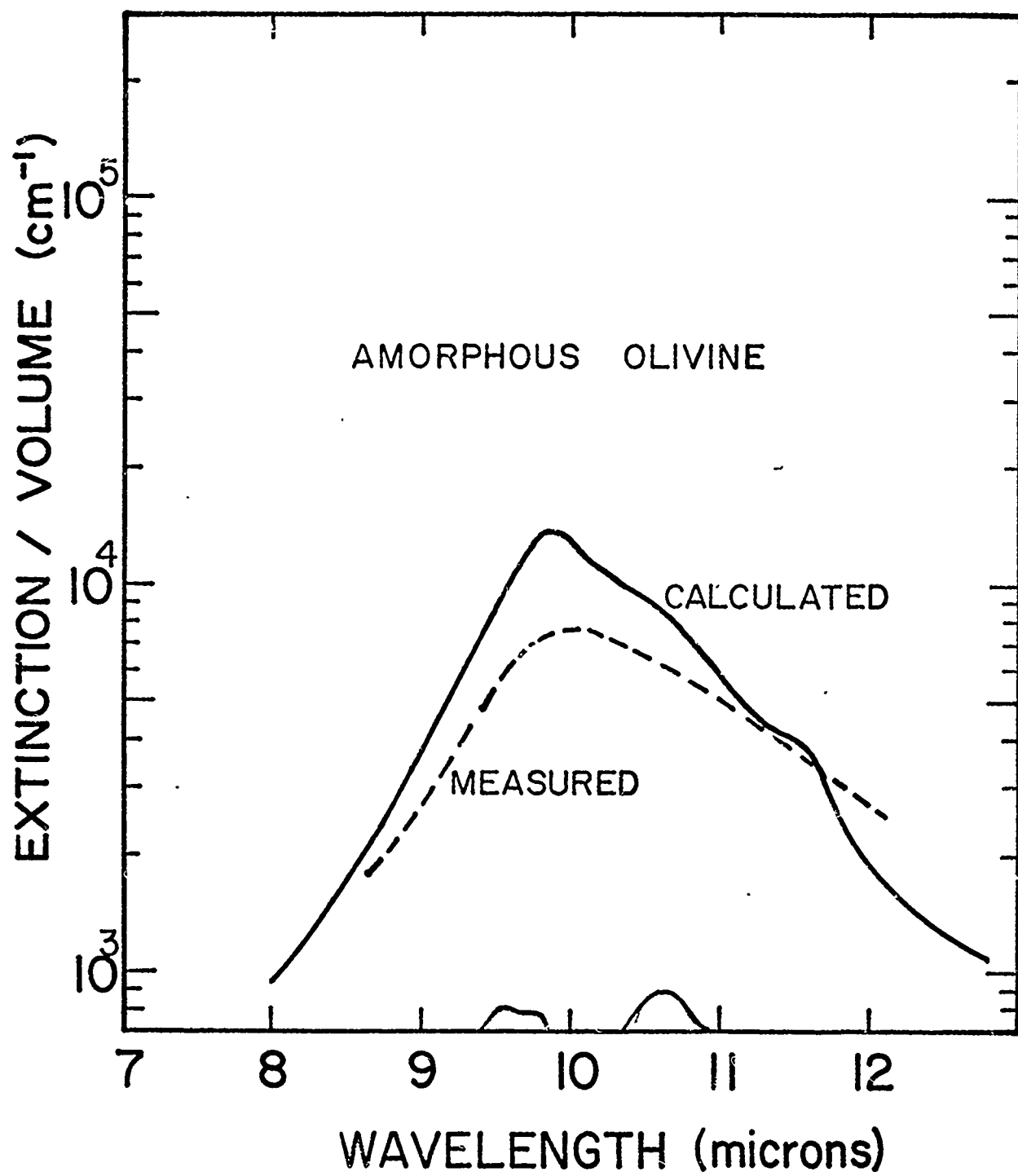


Figure 15

Measured and calculated extinction for amorphous olivine smoke.

theory.

$$\alpha_p = \frac{C_{\text{ext}}}{V} = \frac{2\pi}{\lambda} \frac{\epsilon_2}{\{L_j \epsilon_1 + (1-L_j)\}^2 + (L_j \epsilon_2)^2} \quad (\text{IV-1})$$

The above assumes that the particle is in free space and that scattering is negligible. For a general ellipsoid there are three different L_j 's which are subject to the conditions $0 \leq L_j < 1$ and $\sum L_j = 1$ (see van de Hulst 1957), related to the lengths of the semi-axes. One sees that a resonance occurs in the extinction when

$$L_j \epsilon_1 + (1 - L_j) = 0, \quad (\text{IV-2})$$

the strength of the resonance being stronger as ϵ_2 is smaller. For spheres for which $L_j = 1/3$ for all the axes, the resonance condition is

$$\epsilon_1 = -2.$$

These resonances, which occur at the wavelengths for which $\epsilon_1 = -2$ for spheres and which occur in the negative ϵ_1 region for all shapes, have sometimes been called surface modes. They are probably more correctly termed Fröhlich modes (after Fröhlich 1937). A review with examples is given in Huffman (1977). These modes occur in the vicinity of, but not exactly at, the position of the strong infrared lattice mode resonances. The condition that the strength goes up as ϵ_2 at the Fröhlich mode frequency goes down means that extremely high extinction resonances could occur.

Returning now to the smoke extinction curves of Fig. 14, the three

peaks in the extinction calculations occur at precisely the wavelengths where $\epsilon_1 = -2$ for the three polarization directions of the crystal. This could be determined by a careful comparison of Figs. 11 and 14, but is more clearly shown in Steyer's thesis (1974). The calculated extinction peak of the amorphous smoke (Fig. 15) falls at the wavelength where ϵ_1 is minimum, although it never quite reaches -2 . Because the resonances in ϵ_2 are narrower in the crystalline than they are in the amorphous olivine, the ϵ_2 's at wavelengths where $\epsilon_1 = -2$ are less, giving higher peak efficiencies. Going along with the higher peak efficiencies, however, is the fact that the extinction resonances are much narrower. The appearance of the two extinction spectra are thus considerably different.

In both cases the peak extinction efficiencies are less by a factor of 2 to 4 in the measurements as compared to the calculations. This seems to have been a general trend in the few, previously reported cases in which attempts have been made to compare theoretical and experimental extinctions with no arbitrary scaling (see Steyer et al 1974, and Day 1975). The explanation for the discrepancy seems to lie in the breakdown of the independent sphere approximation for smoke loosely trapped on substrates. Again, Eqs. IV-1 and 2 give some insight into what might happen if two or more particles stick together. They would act somewhat like an elongated particle approximated by different L_j 's, giving Fröhlich modes displaced from the $\epsilon_1 = -2$ wavelength, but still in the negative ϵ_1 region. A distribution of shapes, even if caused by clumping of spheres, should give rise to a broadened extinction band whose maximum is now depressed. This is exactly what one sees in comparing the sphere

calculations and the measurements of Figs. 14 and 15. Even before the smoke particles are trapped on the substrate they form themselves into chains like strings of pearls. This appears to happen in the near vicinity of the arc and prevents the spherical particles from acting independently. An aerosol of the smoke might have slightly higher extinction than when coating a substrate; however, a good guess is that an aerosol of the olivine smoke particles would show extinctions somewhere between the measured and calculated curves, when first produced. After long periods of time, agglomeration of the smoke would likely decrease the volume extinction coefficient even more.

The highest extinctions are seen in the calculations for crystalline smoke, which reach to $4.4 \times 10^4 \text{ cm}^{-1}$ at $11.15 \mu\text{m}$. Although the peaks of the two main absorptions are near to 9.6 and $10.6 \mu\text{m}$ bands, they are not exactly centered on the laser bands. Due to the sharpness of the absorption bands their slight displacement from the desired values produces CO_2 laser extinction values considerably below their peak values. The breadth of the extinction band for amorphous smoke causes it to be almost equally effective in both of the CO_2 bands. Both sets of measurements are accidentally about the same at 9.6 and $10.6 \mu\text{m}$.

V. COMPARISONS AND CONCLUSIONS

Having presented in the above sections the results of extinction for the two bubble materials and the two silicate smokes, it is now possible to give a more educated assessment of which material would provide the more effective extinction agent. The appropriate results were given in Fig. 8 for the bubble materials and Figs. 14 and 15 for the silicate smokes. Amazingly and disgustingly, all four candidates give

about the same extinction within a factor of two. Thus none of the materials are clear choices over the others. Any choice among these would need to be made on other grounds, such as which material is most easy to produce and disperse in practical situations and which aerosol resists agglomeration and settling best.

A significant point regarding the bubbles is that scattering is not the dominant extinction mechanism, so that smaller sized fractions would give more extinction per unit volume of solid. It should also be kept in mind that the extinction per unit volume-of-bubbles would be less than the extinction per unit volume of solid (α_p) discussed in this work. Hence, if a pyrotechnic device had to carry the bubbles already made, as contrasted with materials to make the bubbles from, the appropriate volume extinction coefficient would be less. If on the other hand the weight is the most important parameter in the aerosol producer, it would not matter whether the device carried pre-made bubbles or produced bubbles from bulk material.

In view of the similarity of extinction coefficients derived it appears that other considerations must distinguish between the use of one or the other of these materials. The absorption mechanism responsible for the strong extinction resonances in the silicate smokes could, however, be higher in other materials. Complex optical constants are required before the determination of effectiveness for a given solid can be made.

REFERENCES

- Day, K. L., 1975: Measured extinction of small olivine spheres, Astrophys. J., 199, 660.
- Day, K. L., T. R. Steyer, and D. R. Huffman, 1974: A quantitative study of silicate extinction, Astrophys. J., 191, 415.
- Dave, J. V., 1968: Subroutines for computing the parameters of the electromagnetic radiation scattered by a sphere, IBM Scientific Center, Palo Alto, Calif., Report # 320-3236.
- Debye, P., 1909: Der Lichtdruck auf Kugeln von beliebigem Material, Ann. Phys., 30, 59.
- Glüttler, A., 1952: Ann. Phys. 11, 65.
- Huffman, Donald R., 1977: Interstellar grains: The interaction of light with a small-particle system, Advances in Phys., 26, 129.
- van de Hulst, H. C., 1957: Light scattering by small particles, Wiley.
- Jenkins, F. A., and H. E. White, 1957: Fundamentals of optics, McGraw-Hill, pp. 21-22.
- Kerker, M. 1969: The scattering of light and other electromagnetic radiation, Academic Press.
- Krätschmer, W., and D. R. Huffman, 1978: Infrared extinction of heavy ion irradiated and amorphous olivine with applications to interstellar dust, submitted to Astro. and Space Sci.
- Mie, G., 1908: Beiträge zur Optik trüber Medien, Ann. Phys. 25, 377.
- Steyer, T. R., K. L. Day, and R. R. Huffman, 1974: Infrared absorption by small amorphous quartz spheres, Appl. Opt., 13, 1586.
- Steyer, T. R., 1974: Infrared optical properties of some solids of possible interest in astronomy and astrophysics, Ph.D. Dissertation, Univ. of Arizona.
- Stratton, J. A., 1941: Electromagnetic Theory, McGraw-Hill.
- Sterb, F., 1963: Solid State Physics Vol. 15, Academic Press.